frontiers in Energy Research

ORIGINAL RESEARCH
published: 25 May 2021
doi: 10.3389/fenrg.2021.692059

Improved Photovoltaic Performance of $CsPbI_2Br$ Perovskite Films via Bivalent Metal Chloride Doping

Hong Wei Qiao, Mengjiong Chen, Ziren Zhou, Qilin Cheng, Yu Hou and Hua Gui Yang**

Key Laboratory for Ultrafine Materials of Ministry of Education, Shanghai Engineering Research Center of Hierarchical Nanomaterials, School of Materials Science and Engineering, East China University of Science and Technology, Shanghai, China

Cesium-based all-inorganic perovskite absorbers have attracted increasing attention due to their superior thermal stability, compared to their organic–inorganic counterparts. Up to now, it is a challenge to fabricate high-efficiency all-inorganic perovskite solar cells (PSCs) with low defect densities. Herein, we used bivalent metal chloride salts ($SrCl_2$ and $NiCl_2$) to optimize $CsPbI_2Br$ films. The experimental results indicate that this method could deliver high-quality films with improved electronic property. As a result, the champion device based on the 0.01 M $SrCl_2$–doped $CsPbI_2Br$ film achieved a power conversion efficiency (PCE) of 16.07% with a high open voltage (V_{OC}) of 1,322 mV, which is about 18% higher than that of the pristine device.

Keywords: all-inorganic PSC, $CsPbI_2Br$, bivalent metal chloride salts, doping, PCE

OPEN ACCESS

Edited by:
Xingxing Gu,
Chongqing Technology and Business University, China

Reviewed by:
Xue Lu Wang,
East China Normal University, China
Hua Yu,
Southwest Petroleum University, China
Yu Zhou,
Central South University, China

****Correspondence:***
Yu Hou
yhou@ecust.edu.cn
Hua Gui Yang
hgyang@ecust.edu.cn

Specialty section:
This article was submitted to Electrochemical Energy Conversion and Storage, a section of the journal Frontiers in Energy Research

Received: *07 April 2021*
Accepted: *06 May 2021*
Published: *25 May 2021*

Citation:
Qiao HW, Chen M, Zhou Z, Cheng Q, Hou Y and Yang HG (2021) Improved Photovoltaic Performance of $CsPbI_2Br$ Perovskite Films via Bivalent Metal Chloride Doping. Front. Energy Res. 9:692059. doi: 10.3389/fenrg.2021.692059

INTRODUCTION

Lead halide perovskites are promising photovoltaic materials because of their tunable bandgap, long carrier diffusion length, and easy fabrication (Chen et al., 2015; Shi et al., 2015; Lin et al., 2018; Yang et al., 2019a; Qiao et al., 2019; Fang et al., 2020; Qiao et al., 2020). Unfortunately, the long-term instability of perovskites, especially under thermal conditions, limits the commercial application of PSCs (Yang et al., 2019b; Zhong et al., 2020). All-inorganic cesium lead halide perovskites ($CsPbX_3$, X = Cl, Br, I) have been developed quickly in recent years, whose PCEs have reached 19% with benign thermal endurance (Bai et al., 2018; Wang et al., 2019a; Wang et al., 2019b; Straus et al., 2019; Tan et al., 2019). The $CsPbI_3$ perovskite has a low bandgap of ~1.73 eV but suffers from the intrinsic structural transition from the α-phase to the δ-phase at room temperature (Li et al., 2018; Zeng et al., 2019).

Partial substitution of iodine for bromine anions can effectively stabilize the perovskite structure by tailoring the tolerant factor (Rehman et al., 2017; Fu et al., 2019; Dong et al., 2020). A paradigm is the $CsPbI_2Br$ perovskite with a bandgap of ~1.9 eV and a stable cubic phase at room temperature (Sutton et al., 2016; Yan et al., 2018). However, the PCEs of $CsPbI_2Br$ solar cells were still much lower than those of $CsPbI_3$ devices. Controlling the deposition process of perovskite thin films could optimize film coverage at a long-range scale, as well as reducing the atomic crystal defects (Chen et al., 2019; Duan et al., 2020; Liu et al., 2020). Processing parameters, such as coating speed and annealing temperature, have been initially studied in previous reports (Yu and Gao, 2017; Zhang et al., 2020a). Besides, additives can selectively adsorb on the perovskite surface and regulate perovskite crystallization (Zhang et al., 2019). A number of organic additives, such as dimethylammonium iodide, choline iodine, and dithiocarbamate, have been used to achieve high-quality perovskite films (Yang et al., 2019c; Fu et al., 2020; He et al., 2020). However, inorganic salts have been less investigated in this field, particularly for optimizing the film

morphology and electronic property of all-inorganic perovskites (Wang et al., 2019c; Zhang et al., 2019). Bivalent metal salts are commonly used as inorganic additives to improve films' quality, which is suitable for different organic–inorganic perovskite formulations (Aydin et al., 2019; Wang et al., 2019a). ZnI_2 (Shai et al., 2018) and SnI_2 (Eperon and Ginger, 2017) have been incorporated into organic–inorganic perovskites, which could enhance PCEs of the corresponding PSCs attributed to increased grain size and crystallinity. In addition, the Cl^- ion could passivate grain boundaries and trap defects of perovskite polycrystalline films (Aydin et al., 2019).

Here, we studied the effect of bivalent metal chloride salts ($SrCl_2$ and $NiCl_2$) on the film quality of the $CsPbI_2Br$ perovskite. We revealed that certain amount of metal chloride salts is substantially beneficial for the formation of the perovskite with less trap sites, while excess metal chloride salts are detrimental to the perovskite films. By utilizing $SrCl_2$ dopants, the best planar heterojunction $CsPbI_2Br$ perovskite solar cell achieved a high PCE of 16.07%, with ~18% increment than the pristine one.

EXPERIMENT

Material Preparation

Titanium(IV) chloride ($TiCl_4$, 99%), lead iodide (PbI_2, 99%), cesium iodide (CsI, 99.9%), lead bromide ($PbBr_2$, 98%), bis(trifluoromethane) sulfonimide lithium salt (Li-TFSI, 99.95%), 4-tert-butylpyridine (tBP, 96%), dimethyl sulfoxide (DMSO, 99.8%), and chlorobenzene (99.9%) were purchased from Sigma-Aldrich. Strontium chloride hexahydrate ($SrCl_2.6H_2O$, 99.9%) and nickel chloride hexahydrate ($NiCl_2.6H_2O$, 99.9%) were purchased from Sinopharm Chemical Reagent Co., Ltd. Poly(3-hexylthiophene-2,5-diyl) (P3HT) was purchased from Xi'an Polymer Light Technology Corp. All the chemicals and solvents were used as received without further purification.

Device Fabrication

Fluorine-doped tin oxide (FTO) glasses (Nippon Sheet Glass, 8 Ω/square) were cleaned with soap, acetone, ethanol, and deionized water sequentially for 15 min, respectively. Then, the cleaned FTO glass substrates were treated by a plasma cleaner with O_2 gas for 3 min at middle power radio frequency (10.2 W). Then, the substrates were immersed in a 25 mM $TiCl_4$ aqueous solution for 60 min at 70°C and washed with distilled water and ethanol, followed by annealing at 500°C for 60 min in a muffle oven to form a compact TiO_2 blocking layer. The preparation of $CsPbI_2Br$ films was based on a modified method according to the reported article (Liu et al., 2018). P3HT solution (15 mg/ml in chlorobenzene) as a hole transport layer (HTL) was spin-coated on perovskite films at 2,500 rpm for 30 s, followed by annealing at 120°C for 10 min. Finally, 100 nm-thick Ag was thermally evaporated onto the HTL as a metal electrode. All steps were carried out in a nitrogen glove box (H_2O < 0.01 ppm, O_2 < 0.01 ppm).

Characterization

Field emission scanning electron microscopy (FESEM, HITACHI S4800) was used to characterize the morphology of films. X-ray diffraction (XRD) patterns were acquired by powder X-ray diffraction (PXRD, Bruker Advance D8 X-ray diffractometer Cu Kα radiation, 40 kV). Ultraviolet and visible (UV-Vis) absorption spectrometry was collected using a Cary 500 UV-Vis-NIR spectrophotometer. Photoluminescence (PL) spectra were characterized at room temperature by exciting the sample deposited on the FTO substrate. The excitation wavelength of the Fluorolog-3-p spectrophotometer is 380 nm. The solar cells were illuminated by a solar light simulator (Solar IV-150A, Zolix), and light intensity was calibrated by a standard Newport calibrated KG5-filtered Si reference cell. Current density–voltage (J–V) curves of solar cells were measured by a Keithley 2400 digital source meter under simulated AM 1.5G illumination of 100 mW cm^{-2} with a reverse scan rate of 0.15 V s^{-1}. Solar cells were masked with a metal aperture to define the active area of 0.0625 cm^2. External quantum efficiency (EQE) spectra of solar cells were measured by an SCS10-X150-HBSD system. The electrochemical impedance spectra (EIS) were acquired under an applied voltage of 0–1 V with frequency ranging from 1 Hz to 1 MHz in dark condition. In transient photovoltage (TPV) decay tests, the cells were connected directly in series with an oscilloscope (DSOX3104T), and the input impedance of DSO was 10^6 Ω. An attenuated green laser pulse (DSP-532-A Laser) was used as a small perturbation to the background illumination on the device. The laser-pulse–induced photovoltage variation and the V_{OC} are produced by the background illumination. The wavelength of the laser was 532 nm, the repeating frequency was about 10 Hz, and the pulse width was less than 10 ns.

RESULTS AND DISCUSSION

The deposition of $CsPbI_2Br$ perovskites is based on the spin-coating of perovskite precursors dissolved in DMSO solution. We firstly included $SrCl_2$ into perovskite precursor solution in the concentrations of 0.005, 0.01, and 0.05 M, respectively. The morphological characteristics of $CsPbI_2Br$ films were firstly visualized by SEM characterizations. As shown in **Figure 1A**, the pristine film presents a non-flat surface with a high coverage. By the addition of 0.005–0.01 M $SrCl_2$, the $CsPbI_2Br$ films retained the fully covered morphology (**Figures 1B,C**). For the film with 0.05 M $SrCl_2$ (**Figure 1D**), a rough surface with many pinholes was observed, implying the adverse effect of excess $SrCl_2$ on film formation.

We also noted that the 0.05 M $SrCl_2$–doped films degraded rapidly in ambient condition. XRD patterns in **Figure 2A** disclose the non-perovskite phase of the doped film with 0.05 M $SrCl_2$. Although the ionic radius of Sr^{2+} (118 pm) is similar to that of Pb^{2+} (119 pm) (Shannon, 1976), we still infer that excess metal dopants would favor the formation of non-perovskite phases (Phung et al., 2020). An intriguing phenomenon is that the full width at half maximum (FWHM) of the (100) diffraction peak reduces from 0.161 of pristine to 0.139 of film with 0.01 M $SrCl_2$. The narrowed XRD diffraction peak signifies the enhanced crystallinity with less crystal defects (Li et al., 2020). Therefore, we conclude that the $SrCl_2$ additive is a double-edged sword for the perovskite: low concentration of $SrCl_2$ can promote the formation, while high concentration can generate the

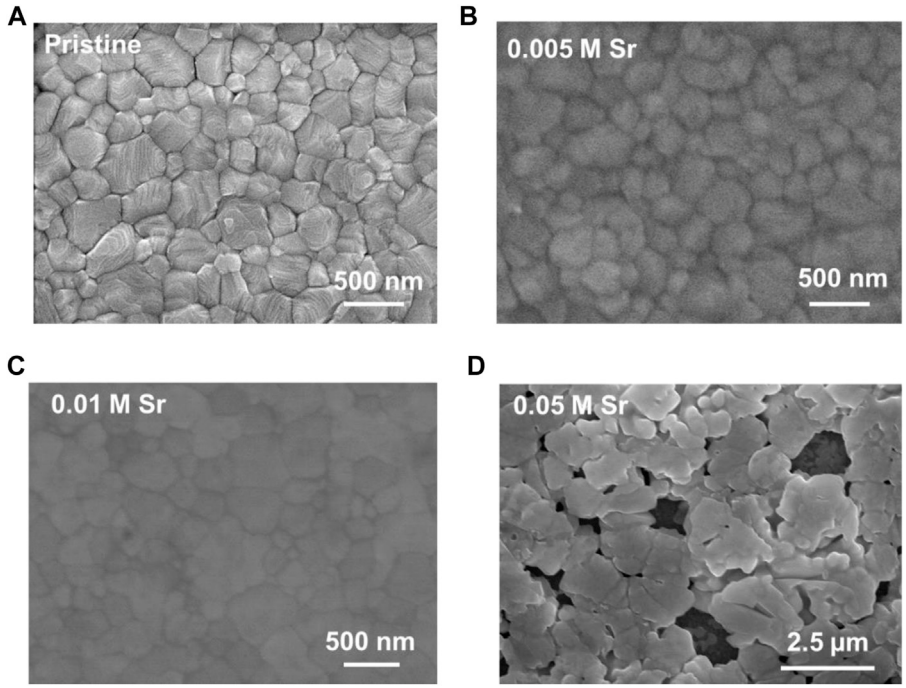

FIGURE 1 | Top-view SEM images of **(A)** pristine, **(B)** 0.005 M $SrCl_2$–doped, **(C)** 0.01 M $SrCl_2$–doped, and **(D)** 0.05 M $SrCl_2$–doped $CsPbI_2Br$ films.

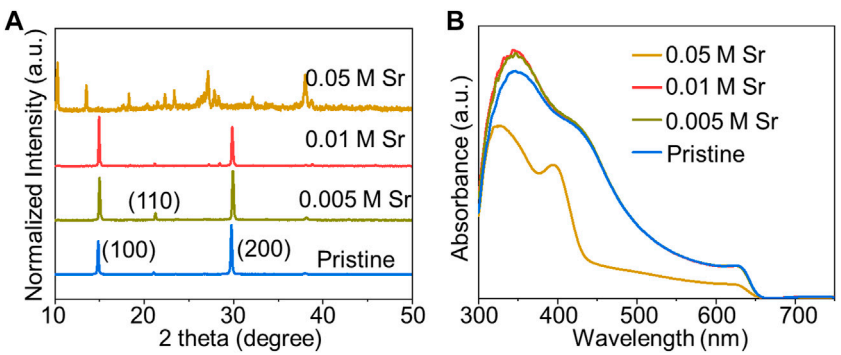

FIGURE 2 | (A) XRD patterns and **(B)** UV-Vis spectra of $CsPbI_2Br$ films with different dopant concentrations of $SrCl_2$ deposited on compact TiO_2/FTO.

non-perovskite structure. The identical trend was also observed in the UV-Vis spectra in **Figure 2B**.

To further examine the effect of bivalent metal chlorides on $CsPbI_2Br$ perovskite films, we used $NiCl_2$ as an additive into perovskite films. The concentration of $NiCl_2$ is 0.01 M for all samples, which corresponds to 0.83% of the molar ratio with Pb ions. As expected, the $NiCl_2$-doped sample exhibits smooth and uniform morphology (**Figure 3**). XRD patterns in **Figure 4A** further ascertain the cubic perovskite phase of all samples. Absorbance offsets of films were determined to be ~650 nm by UV-Vis spectra in **Figure 4B**. Steady-state PL spectra were operated to assess the photoelectrical property of perovskite films deposited on glass substrates. As shown in **Figure 4C**, the PL intensities of $SrCl_2$- and $NiCl_2$-doped perovskite films are 4.46 and 2.72 times higher than that of the pristine film, respectively, indicating mitigated non-radiative recombination in bivalent metal chloride–doped films (Han et al., 2016; You et al., 2018).

We then measured the *J–V* characteristics of as-prepared solar cells. Solar cells were fabricated with a planar n-i-p configuration of FTO/compact-TiO_2 (c-TiO_2)/$CsPbI_2Br$/P3HT/Au (**Figure 5A**). All *J–V* characteristics were measured under simulated AM 1.5G illumination with a reverse scan rate of 0.15 V s^{-1}. As shown in **Figure 5B** and **Table 1**, the pristine device shows a short-circuit current density (J_{SC}) of 15.28 mA cm^{-2}, an open-circuit voltage (V_{OC}) of 1,197 mV, a fill factor (FF) of 0.71%, and a PCE of 12.89%. The addition of $SrCl_2$ mainly enhances the V_{OC} values of devices: the V_{OC} are 1,266, 1,278, 1,278, and 1,163 mV, by using 0.001, 0.005, 0.01, and 0.05 M $SrCl_2$ additives. The champion doped device was obtained by

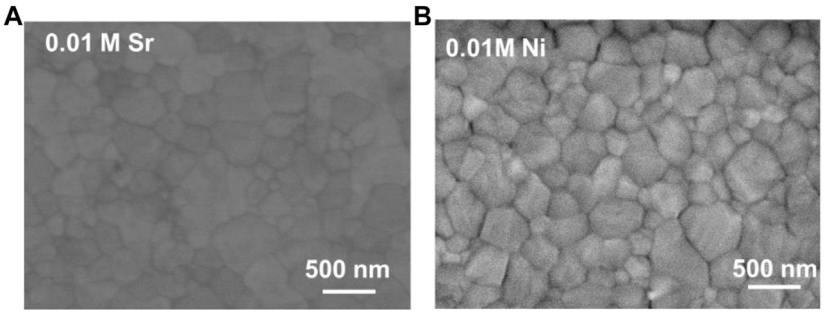

FIGURE 3 | Top-view SEM images of **(A)** 0.01 M $SrCl_2$–doped and **(B)** 0.01 M $NiCl_2$–doped $CsPbI_2Br$ films.

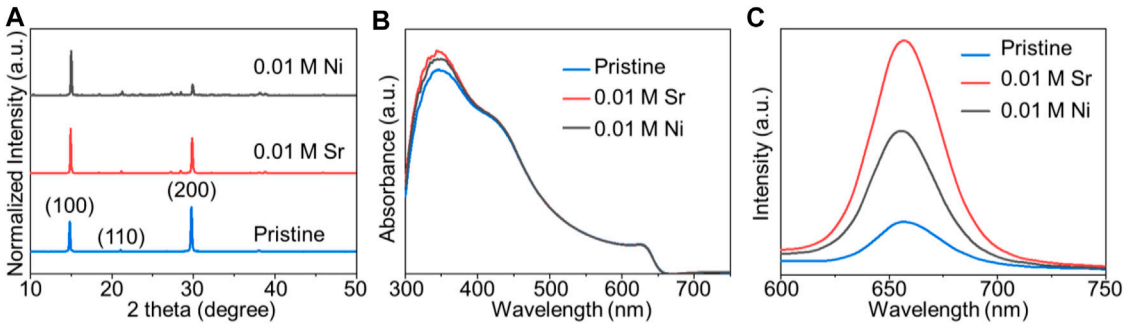

FIGURE 4 | (A) XRD patterns and **(B)** UV-Vis spectra of the pristine, 0.01 M $SrCl_2$–doped, and 0.01 M $NiCl_2$–doped $CsPbI_2Br$ thin films on compact TiO_2/FTO. **(C)** Photoluminescence (PL) spectra of the pristine, 0.01 M $SrCl_2$–doped, and 0.01 M $NiCl_2$–doped $CsPbI_2Br$ thin films deposited on glass.

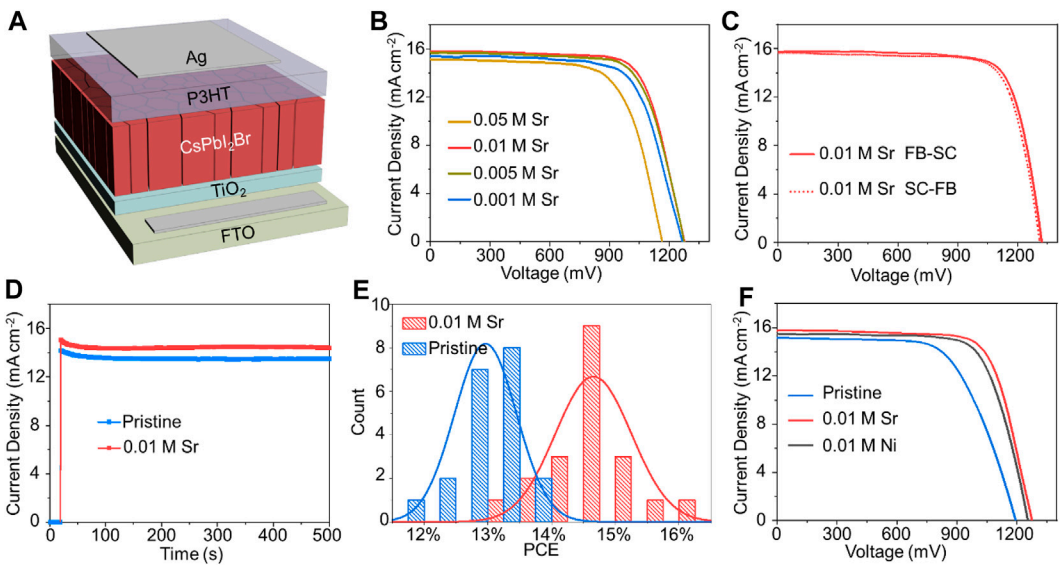

FIGURE 5 | (A) Device architecture of a typical PSC device. **(B)** *J–V* curves of PSCs based on $SrCl_2$-doped $CsPbI_2Br$ films with different dopant concentrations. **(C)** *J–V* curves of the champion device for the $SrCl_2$-doped PSC scanned from forward bias (FB) to short circuit (SC) and SC to FB with a scan rate of 0.15 V s^{-1}. **(D)** Photocurrent density as a function of time for a device held at the maximum power point. **(E)** Statistical distribution of PCEs of 20 individual PSCs based on pristine and 0.01 M $SrCl_2$–doped $CsPbI_2Br$ films. **(F)** *J–V* curves of typical devices under simulated AM 1.5G illumination of 100 mW cm^{-2} for pristine, 0.01 M $SrCl_2$–doped, and 0.01 M $NiCl_2$–doped $CsPbI_2Br$ cells.

TABLE 1 | Photovoltaic parameters of PSCs with different $SrCl_2$ dopant concentrations under simulated AM 1.5G of 100 mW/cm^2 solar irradiation.

Sample	J_{SC} (mA cm^{-2})	V_{OC} (mV)	FF	PCE (%)
Pristine	15.28	1,197	0.71	12.89
0.001 M $SrCl_2$	15.37	1,266	0.70	13.55
0.005 M $SrCl_2$	15.64	1,278	0.72	14.32
0.01 M $SrCl_2$	15.67	1,278	0.73	14.61
0.05 M $SrCl_2$	15.02	1,163	0.70	12.11

TABLE 2 | Summary of photovoltaic performance for champion devices (FB–SC and SC–FB) based on the 0.01 M $SrCl_2$–doped perovskite film.

Direction	J_{SC} (mA cm^{-2})	V_{OC} (mV)	FF	PCE (%)
FB–SC	15.75	1,322	0.77	16.07
SC–FB	15.66	1,312	0.77	15.73

using 0.01 M $SrCl_2$ with a J_{SC} of 15.75 mA cm^{-2}, a V_{OC} of 1,322 mV, a FF of 0.77, and a PCE of 16.07% under reverse scan condition (**Figure 5C** and **Table 2**). Notably, negligible hysteresis was observed for this champion device. In contrast, the best pristine sample exhibited a J_{SC} of 15.69 mA cm^{-2}, a V_{OC} of 1,217 mV, a FF of 0.73, and a PCE of 13.66% under reverse scan condition (**Supplementary Figure S1** and **Supplementary Table S1**). We then held these devices under maximum power point (MPP) to measure the stabilized power output, as shown in **Figure 5D** and **Supplementary Figure S2**. The current density at the MPP was 14.39 mA cm^{-2} at a bias voltage of 1,100 mV, corresponding to an efficiency of 15.83%. The current density at the MPP was 13.47 mA cm^{-2} at a bias voltage of 960 mV, corresponding to an efficiency of 12.93%. **Supplementary Figure S3** exhibits the external quantum efficiency (EQE) spectra of PSCs. The integration of the EQE spectrum yields the photocurrent of 15.37 mA cm^{-2} for the 0.01 M $SrCl_2$–doped device and 15.24 mA cm^{-2} for the pristine device, which are consistent with the corresponding *J–V* measurements shown in **Figure 5C** and **Supplementary Figure S1**.

A statistical analysis of 20 individual devices reveals the good productivity of $SrCl_2$-doped devices such that the mean PCEs of pristine and $SrCl_2$-doped devices are 14.66 and 12.96%, respectively (**Figure 5E**). Moreover, inclusion of $NiCl_2$ also improved the device performance significantly (**Figure 5F** and **Supplementary Table S2**). The V_{OC} of the $NiCl_2$-doped device increased to 1,245 mV, yielding a PCE of 13.83%. The results presented herein manifest our strategy as versatile and universal with a large variety of possible metal salts for perovskite devices.

We then studied the optical and electrical properties of the doped perovskite devices to probe the origin for performance enhancement. EIS spectra were operated to characterize the carrier behaviors of as-fabricated $CsPbI_2Br$ devices, and the equivalent circuit model (Cui et al., 2020; Zhang et al., 2020b) is displayed in **Figure 6A**. The charge recombination resistance (R_{rec}) of the $SrCl_2$-doped device is much higher than that of the pristine device at a bias of 0.8 V (**Figure 6A**). The R_{rec} values of the $SrCl_2$-doped device are about one time larger than R_{rec} values of the pristine one under the bias range of 0–1 V, which confirms the longer carrier lifetime of the $SrCl_2$-doped device (**Figure 6B**) (Quilettes et al., 2015). We further investigated charge-transport properties of PSCs with and without $SrCl_2$ by using TPV measurements. The TPV curve revealed that incorporation of $SrCl_2$ increased the charge-carrier lifetime (**Figure 6C**), indicating a decrease in the undesired charge-carrier recombination (Seitkhan et al., 2020). As shown in **Supplementary Figure S4**, the ideality factor (m) was measured to evaluate the recombination process in PSCs. The value of m for $SrCl_2$-doped devices (1.31 kT/e) is smaller than 1.74 kT/e of the pristine device, illustrating the reduced trap-assisted charge recombination, where K is the Boltzmann constant, T is an absolute temperature of 300 K, and e is the elementary charge (Aydin et al., 2019; Dong et al., 2021).

CONCLUSION

In summary, we report a simple strategy to modulate the $CsPbI_2Br$ perovskite by using bivalent metal chloride additives, which facilitates the formation of high-quality perovskite films. A high PCE of 16.07% was achieved on solar cells by $SrCl_2$ doping, which could eliminate defective trap states and extend carrier lifetime. Our strategy would provide new insights into controllably fabricating high-efficiency all-inorganic perovskite solar cells.

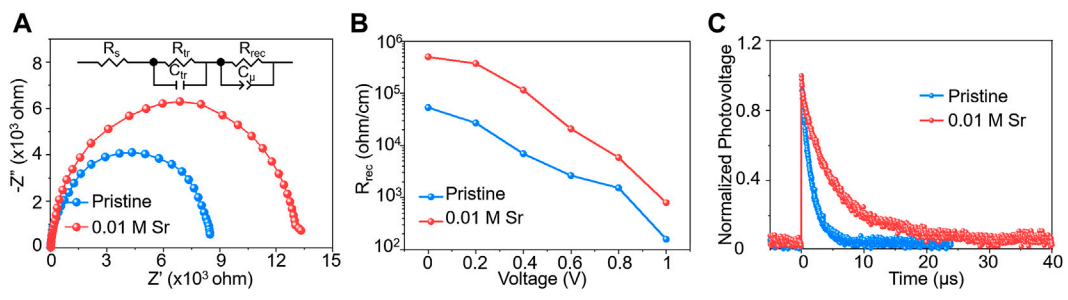

FIGURE 6 | (A) Nyquist plots of the PSCs based on pristine and 0.01 M $SrCl_2$–doped $CsPbI_2Br$ films recorded at 0.8 V in dark condition. **(B)** R_{rec} of PSCs based on pristine and 0.01 M $SrCl_2$–doped $CsPbI_2Br$ films measured at different applied bias voltages. **(C)** TPV measurements of $CsPbI_2Br$ cells with and without $SrCl_2$ dopants.

DATA AVAILABILITY STATEMENT

The original contributions presented in the study are included in the article/**Supplementary Material**, and further inquiries can be directed to the corresponding authors.

AUTHOR CONTRIBUTIONS

HY and YH conceived the project and contributed to the design of the experiments and analysis of the data. HQ performed the material preparation, device fabrication, and characterizations and wrote the manuscript with the help of HY, YH, MC, ZZ, and QC coordinated this research. All authors contributed to the scientific discussion and manuscript revisions.

FUNDING

This work was financially supported by the National Natural Science Foundation of China (51972111), National Ten Thousand Talents Program for Young Top-Notch Talent, National Natural Science Fund for Distinguished Young Scholars (51725201), International (Regional) Cooperation and Exchange Projects of the National Natural Science Foundation of China (51920105003), Innovation Program of Shanghai Municipal Education Commission (E00014), Fundamental Research Funds for the Central Universities (JKD012016025), and Shanghai Engineering Research Center of Hierarchical Nanomaterials (18DZ2252400).

ACKNOWLEDGMENTS

The authors thank the Frontiers Science Center for Materiobiology and Dynamic Chemistry for providing some facilities to carry out this work.

SUPPLEMENTARY MATERIAL

The Supplementary Material for this article can be found online at: https://www.frontiersin.org/articles/10.3389/fenrg.2021.692059/full#supplementary-material

REFERENCES

Aydin, E., Bastiani, M., and Wolf, S. (2019). Defect and Contact Passivation for Perovskite Solar Cells. *Adv. Mater.* 31, e1900428. doi:10.1002/adma.201900428

Bai, D., Zhang, J., Jin, Z., Bian, H., Wang, K., Wang, H., et al. (2018). Interstitial Mn2+-Driven High-Aspect-Ratio Grain Growth for Low-Trap-Density Microcrystalline Films for Record Efficiency CsPbI2Br Solar Cells. *ACS Energy Lett.* 3, 970–978. doi:10.1021/acsenergylett.8b00270

Chen, W., Chen, H., Xu, G., Xue, R., Wang, S., Li, Y., et al. (2019). Precise Control of Crystal Growth for Highly Efficient $CsPbI_2Br$ Perovskite Solar Cells. *Joule* 3, 191–204. doi:10.1016/j.joule.2018.10.011

Chen, W., Wu, Y., Yue, Y., Liu, J., Zhang, W., Yang, X., et al. (2015). Efficient and Stable Large-Area Perovskite Solar Cells with Inorganic Charge Extraction Layers. *Science* 350, 944–948. doi:10.1126/science.aad1015

Cui, X., Chen, Y., Zhang, M., Harn, Y. W., Qi, J., Gao, L., et al. (2020). Tailoring Carrier Dynamics in Perovskite Solar Cells via Precise Dimension and Architecture Control and Interfacial Positioning of Plasmonic Nanoparticles. *Energy Environ. Sci.* 13, 1743–1752. doi:10.1039/C9EE03937F

deQuilettes, D. W., Vorpahl, S. M., Stranks, S. D., Nagaoka, H., Eperon, G. E., Ziffer, M. E., et al. (2015). Solar Cells Impact of Microstructure on Local Carrier Lifetime in Perovskite Solar Cells. *Science* 348, 683–686. doi:10.1126/science.aaa5333

Dong, H., Zhang, C., Liu, X., Yao, J., and Zhao, Y. S. (2020). Materials Chemistry and Engineering in Metal Halide Perovskite Lasers. *Chem. Soc. Rev.* 49, 951–982. doi:10.1039/C9CS00598F

Dong, W., Xiong, S., Yang, J., Qiao, W., Zeng, Q., Wang, X., et al. (2021). Black Phosphorus Doped Poly(triarylamine) as Hole Transport Layer for Highly Efficient Perovskite Solar Cells. *Org. Electron.* 89, 106052. doi:10.1016/j.orgel.2020.106052

Duan, C., Cui, J., Zhang, M., Han, Y., Yang, S., Zhao, H., et al. (2020). Precursor Engineering for Ambient-Compatible Antisolvent-Free Fabrication of High-Efficiency $CsPbI_2Br$ Perovskite Solar Cells. *Adv. Energy Mater.* 10, 2000691. doi:10.1002/aenm.202000691

Eperon, G. E., and Ginger, D. S. (2017). B-site Metal Cation Exchange in Halide Perovskites. *ACS Energy Lett.* 2, 1190–1196. doi:10.1021/acsenergylett.7b00290

Fang, T., Wang, T., Li, X., Dong, Y., Bai, S., and Song, J. (2020). Perovskite QLED with an External Quantum Efficiency of over 21% by Modulating Electronic Transport. *Sci. Bull.* 66, 36–43. doi:10.1016/j.scib.2020.08.025

Fu, S., Zhang, W., Li, X., Wan, L., Wu, Y., Chen, L., et al. (2020). Dual-Protection Strategy for High-Efficiency and Stable $CsPbI_2Br$ Inorganic Perovskite Solar Cells. *ACS Energy Lett.* 5, 676–684. doi:10.1021/acsenergylett.9b02716

Fu, Y., Zhu, H., Chen, J., Hautzinger, M. P., Zhu, X.-Y., and Jin, S. (2019). Metal Halide Perovskite Nanostructures for Optoelectronic Applications and the Study of Physical Properties. *Nat. Rev. Mater.* 4, 169–188. doi:10.1038/s41578-019-0080-9

Han, Q., Bae, S.-H., Sun, P., Hsieh, Y.-T., Yang, Y. M., Rim, Y. S., et al. (2016). Single Crystal Formamidinium Lead Iodide ($FAPbI_3$): Insight into the Structural, Optical, and Electrical Properties. *Adv. Mater.* 28, 2253–2258. doi:10.1002/adma.201505002

He, J., Liu, J., Hou, Y., Wang, Y., Yang, S., and Yang, H. G. (2020). Surface Chelation of Cesium Halide Perovskite by Dithiocarbamate for Efficient and Stable Solar Cells. *Nat. Commun.* 11, 4237. doi:10.1038/s41467-020-18015-5

Li, B., Zhang, Y., Fu, L., Yu, T., Zhou, S., Zhang, L., et al. (2018). Surface Passivation Engineering Strategy to Fully-Inorganic Cubic $FaPbI_3$ Perovskites for High-Performance Solar Cells. *Nat. Commun.* 9, 1076. doi:10.1038/s41467-018-03169-0

Li, C., Pan, Y., Hu, J., Qiu, S., Zhang, C., Yang, Y., et al. (2020). Vertically Aligned 2D/3D Pb-Sn Perovskites with Enhanced Charge Extraction and Suppressed Phase Segregation for Efficient Printable Solar Cells. *ACS Energy Lett.* 5, 1386–1395. doi:10.1021/acsenergylett.0c00634

Lin, K., Xing, J., Quan, L. N., de Arquer, F. P. G., Gong, X., Lu, J., et al. (2018). Perovskite Light-Emitting Diodes with External Quantum Efficiency Exceeding 20 Per Cent. *Nature* 562, 245–248. doi:10.1038/s41586-018-0575-3

Liu, C., Li, W., Zhang, C., Ma, Y., Fan, J., and Mai, Y. (2018). All-Inorganic $CsPbI_2Br$ Perovskite Solar Cells with High Efficiency Exceeding 13. *J. Am. Chem. Soc.* 140, 3825–3828. doi:10.1021/jacs.7b13229

Liu, C., Yang, Y., Syzgantseva, O. A., Ding, Y., Syzgantseva, M. A., Zhang, X., et al. (2020). α-$CsPbI_3$ Bilayers via One-Step Deposition for Efficient and Stable All-Inorganic Perovskite Solar Cells. *Adv. Mater.* 32, 2002632. doi:10.1002/adma.202002632

Phung, N., Félix, R., Meggiolaro, D., Al-Ashouri, A., Sousa e Silva, G., Hartmann, C., et al. (2020). The Doping Mechanism of Halide Perovskite Unveiled by Alkaline Earth Metals. *J. Am. Chem. Soc.* 142, 2364–2374. doi:10.1021/jacs.9b11637

Qiao, H. W., Yang, S., Wang, Y., Chen, X., Wen, T. Y., Tang, L. J., et al. (2019). A Gradient Heterostructure Based on Tolerance Factor in High-Performance Perovskite Solar Cells with 0.84 Fill Factor. *Adv. Mater.* 31, 1804217. doi:10.1002/adma.201804217

Qiao, W.-C., Wu, J., Zhang, R., Ou-Yang, W., Chen, X., Yang, G., et al. (2020). *In Situ* NMR Investigation of the Photoresponse of Perovskite crystal. *Matter* 3, 2042–2054. doi:10.1016/j.matt.2020.09.004

Rehman, W., McMeekin, D. P., Patel, J. B., Milot, R. L., Johnston, M. B., Snaith, H. J., et al. (2017). Photovoltaic Mixed-Cation lead Mixed-Halide Perovskites: Links between Crystallinity, Photo-Stability and Electronic Properties. *Energy Environ. Sci.* 10, 361–369. doi:10.1039/C6EE03014A

Seitkhan, A., Neophytou, M., Hallani, R. K., Troughton, J., Gasparini, N., Faber, H., et al. (2020). A Multilayered Electron Extracting System for Efficient Perovskite Solar Cells. *Adv. Funct. Mater.* 30, 2004273. doi:10.1002/adfm.202004273

Shai, X., Wang, J., Sun, P., Huang, W., Liao, P., Cheng, F., et al. (2018). Achieving Ordered and Stable Binary Metal Perovskite via Strain Engineering. *Nano Energy* 48, 117–127. doi:10.1016/j.nanoen.2018.03.047

Shannon, R. D. (1976). Revised Effective Ionic Radii and Systematic Studies of Interatomic Distances in Halides and Chalcogenides. *Acta Cryst. Sect A.* 32, 751–767. doi:10.1107/S0567739476001551

Shi, D., Adinolfi, V., Comin, R., Yuan, M., Alarousu, E., Buin, A., et al. (2015). Low Trap-State Density and Long Carrier Diffusion in Organolead Trihalide Perovskite Single Crystals. *Science* 347, 519–522. doi:10.1126/science.aaa2725

Straus, D. B., Guo, S., and Cava, R. J. (2019). Kinetically Stable Single Crystals of Perovskite-phase $CsPbI_3$. *J. Am. Chem. Soc.* 141, 11435–11439. doi:10.1021/jacs.9b06055

Sutton, R. J., Eperon, G. E., Miranda, L., Parrott, E. S., Kamino, B. A., Patel, J. B., et al. (2016). Bandgap-Tunable Cesium Lead Halide Perovskites with High Thermal Stability for Efficient Solar Cells. *Adv. Energy Mater.* 6, 1502458. doi:10.1002/aenm.201502458

Tan, Q., Ye, G., Zhang, Y., Du, X., Liu, H., Xie, L., et al. (2019). Vacuum-filtration Enabled Large-Area $CsPbBr_3$ Films on Porous Substrates for Flexible Photodetectors. *J. Mater. Chem. C* 7, 13402–13409. doi:10.1039/C9TC04032C

Wang, K., Subhani, W. S., Wang, Y., Zuo, X., Wang, H., Duan, L., et al. (2019a). Metal Cations in Efficient Perovskite Solar Cells: Progress and Perspective. *Adv. Mater.* 31, 1902037. doi:10.1002/adma.201902037

Wang, Y., Dar, M. I., Ono, L. K., Zhang, T., Kan, M., Li, Y., et al. (2019b). Thermodynamically Stabilized β-$CsPbI_3$-based Perovskite Solar Cells with Efficiencies >18. *Science* 365, 591–595. doi:10.1126/science.aav8680

Wang, Y., Liu, X., Zhang, T., Wang, X., Kan, M., Shi, J., et al. (2019c). The Role of Dimethylammonium Iodide in $CsPbI_3$ Perovskite Fabrication: Additive or Dopant? *Angew. Chem. Int. Ed.* 58, 16691–16696. doi:10.1002/anie.201910800

Yan, L., Xue, Q., Liu, M., Zhu, Z., Tian, J., Li, Z., et al. (2018). Interface Engineering for All-Inorganic $CsPbI_2Br$ Perovskite Solar Cells with Effciency over 14%. *Adv. Mater.* 30, 1802509. doi:10.1002/adma.201802509

Yang, S., Chen, S., Mosconi, E., Fang, Y., Xiao, X., Wang, C., et al. (2019a). Stabilizing Halide Perovskite Surfaces for Solar Cell Operation with Wide-Bandgap lead Oxysalts. *Science* 365, 473–478. doi:10.1126/science.aax3294

Yang, S., Dai, J., Yu, Z., Shao, Y., Zhou, Y., Xiao, X., et al. (2019b). Tailoring Passivation Molecular Structures for Extremely Small Open-Circuit Voltage Loss in Perovskite Solar Cells. *J. Am. Chem. Soc.* 141, 5781–5787. doi:10.1021/jacs.0c0642110.1021/jacs.8b13091

Yang, Z., Yu, Z., Wei, H., Xiao, X., Ni, Z., Chen, B., et al. (2019c). Enhancing Electron Diffusion Length in Narrow-Bandgap Perovskites for Efficient Monolithic Perovskite Tandem Solar Cells. *Nat. Commun.* 10, 4498. doi:10.1038/s41467-019-12513-x

You, S., Wang, H., Bi, S., Zhou, J., Qin, L., Qiu, X., et al. (2018). A Biopolymer Heparin Sodium Interlayer Anchoring TiO2 and $MAPbI_3$ Enhances Trap Passivation and Device Stability in Perovskite Solar Cells. *Adv. Mater.* 30, 1706924. doi:10.1002/adma.201706924

Yu, Y., and Gao, P. (2017). Development of Electron and Hole Selective Contact Materials for Perovskite Solar Cells. *Chin. Chem. Lett.* 28, 1144–1152. doi:10.1016/j.cclet.2017.04.020

Zeng, Q., Zhang, X., Liu, C., Feng, T., Chen, Z., Zhang, W., et al. (2019). Inorganic $CsPbI_2Br$ Perovskite Solar Cells: The Progress and Perspective. *Sol. RRL* 3, 1800239. doi:10.1002/solr.201800239

Zhang, C., Wang, K., Wang, Y., Subhani, W. S., Jiang, X., Wang, S., et al. (2020a). Low-Temperature Crystallization of $CsPbIBr_2$ Perovskite for High Performance Solar Cells. *Sol. RRL* 4, 2000254. doi:10.1002/solr.202000254

Zhang, J., Hodes, G., Jin, Z., and Liu, S. (2019). All-Inorganic CsPbX 3 Perovskite Solar Cells: Progress and Prospects. *Angew. Chem. Int. Ed.* 58, 15596–15618. doi:10.1002/anie.201901081

Zhang, S., Si, H., Fan, W., Shi, M., Li, M., Xu, C., et al. (2020b). Graphdiyne: Bridging SnO_2 and Perovskite in Planar Solar Cells. *Angew. Chem. Int. Ed.* 59, 11573–11582. doi:10.1002/ange.20200350210.1002/anie.202003502

Zhong, J. X., Wu, W. Q., Ding, L., and Kuang, D. B. (2020). Blade-coating Perovskite Films with Diverse Compositions for Efficient Photovoltaics. *Energy Environ. Mater.* doi:10.1002/eem2.12118

Conflict of Interest: The authors declare that the research was conducted in the absence of any commercial or financial relationships that could be construed as a potential conflict of interest.